

The Pivotal Role of Symmetry in the Ruthenium-Catalyzed Ring-Closing Metathesis of Olefins

Chiara Costabile,^[a] Annalisa Mariconda,^[a] Luigi Cavallo,^[a] Pasquale Longo,^[a]
Valerio Bertolasi,^[b] Francesco Ragone,^[a] and Fabia Grisi*^[a]

Abstract: The synthesis of Ru-based precatalysts with N-heterocyclic carbene (NHC) ligands bearing *syn*- and *anti*-methyl groups on the NHC backbone and aryl N-substituents with differing steric bulk was carried out. The catalytic behavior of the monophosphine Ru precatalysts (**7a**, **7b**, **8a**, and **8b**) was compared to the corresponding family of phosphine-free catalysts (**9a**, **9b**, **10a** and **10b**) in the ring-closing metathesis (RCM) of olefins. These

catalysts showed high efficiency in RCM reactions and the *syn*-isomers **7a** and **9a**, in particular, proved to be among the most active catalysts in the formation of tetrasubstituted olefins through RCM. DFT studies on the

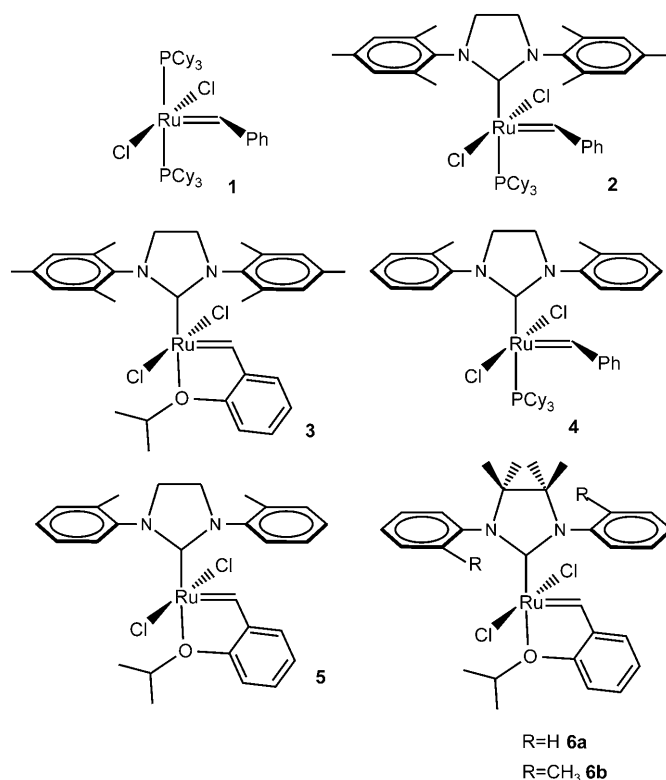
entire RCM catalytic cycle of hindered olefins were performed to rationalize the different behaviors of catalysts with *syn*- and *anti*-methyl groups on the NHC backbone. Theoretical results not only disclosed how NHC symmetry influences the overall activity of the catalyst, but also gave relevant and more general indications on the crucial steps of the RCM of olefins.

Keywords: density functional calculations • metathesis • N-heterocyclic carbenes • ring-closing metathesis • ruthenium

Introduction

Olefin metathesis represents one of the most attractive and valuable tools for the formation of carbon-carbon double bonds. With the advent of efficient Ru-carbene complexes that combine ease of use (remarkable air and moisture stability) and excellent compatibility with a wide range of functional groups, a variety of applications such as ring-closing metathesis (RCM), cross metathesis (CM), ring-opening metathesis polymerization (ROMP), ring-opening cross metathesis (ROCM), acyclic diene metathesis polymerization (ADMET), and enyne metathesis have been developed.^[1,2]

In particular, RCM has gained enormous importance in organic synthesis as an indispensable means to generate carbo- and heterocycles.^[3] Since the discovery of well defined Ru-alkylidene olefin metathesis catalysts (e.g., Grubbs first-generation catalyst **1**),^[4] a lot of attention has



[a] Dr. C. Costabile, Dr. A. Mariconda, Prof. Dr. L. Cavallo, Prof. P. Longo, Dr. F. Ragone, Dr. F. Grisi
Dipartimento di Chimica e Biologia
Università degli Studi di Salerno
Via Ponte Don Melillo, 84084 Fisciano, Salerno (Italy)
Fax: (+39)089969603
E-mail: fgrisi@unisa.it

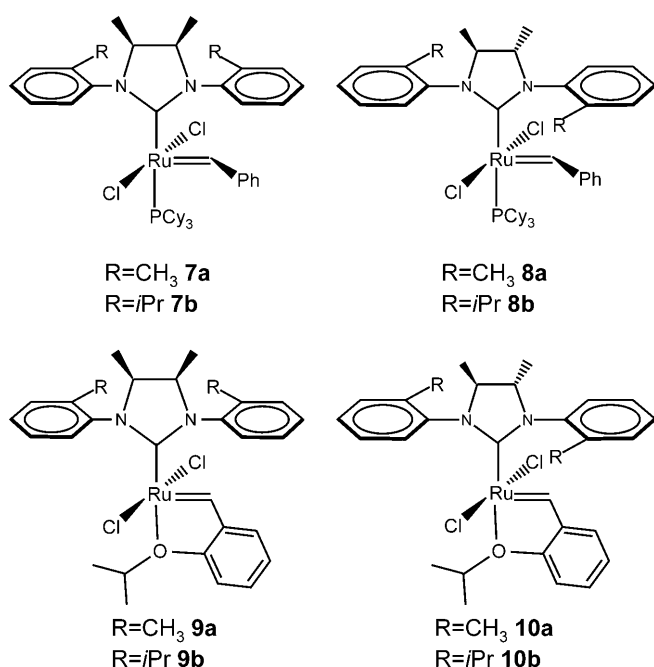
[b] Prof. V. Bertolasi
Dipartimento di Chimica and
Centro di Strutturistica Diffraattometrica
Università di Ferrara
Via L. Borsari 46, 44100 Ferrara (Italy)

Supporting information for this article is available on the WWW under <http://dx.doi.org/10.1002/chem.201100483>.

been given to designing new Ru-based catalysts with improved applicability. Major achievements have been attained by replacing one phosphine in first-generation catalysts by a

N-heterocyclic carbene (NHC) ligand (e.g., second-generation catalyst **2**)^[5] as well as by designing catalysts containing a chelating ether moiety (e.g., Hoveyda–Grubbs second-generation catalyst **3**).^[6] To further improve catalyst activity, stability, and selectivity, and to consequently extend the scope of olefin metathesis, intensive research efforts have been directed toward the modification of the NHC ligand.^[7,8] Grubbs et al. recently reported that small variations of the NHC aryl N-substituents and/or backbone substitution (e.g., complexes **4**, **5**, and **6**) increases catalytic efficiency, particularly in the challenging RCM of hindered substrates. The emerging idea is that a reduction of the bulkiness of the N-substituents results in better catalytic activity, while NHC backbone substitution improves catalyst stability.^[9–12]

Recently, we focused on the synthesis and reactivity of NHC Ru complexes bearing *syn*- and *anti*-methyl groups on the backbone and various N-substituents.^[13,14] We have found that precatalysts with *o*-tolyl N-substituents (**7a** and **8a**) show high efficiency in RCM. Moreover, the *syn* isomer

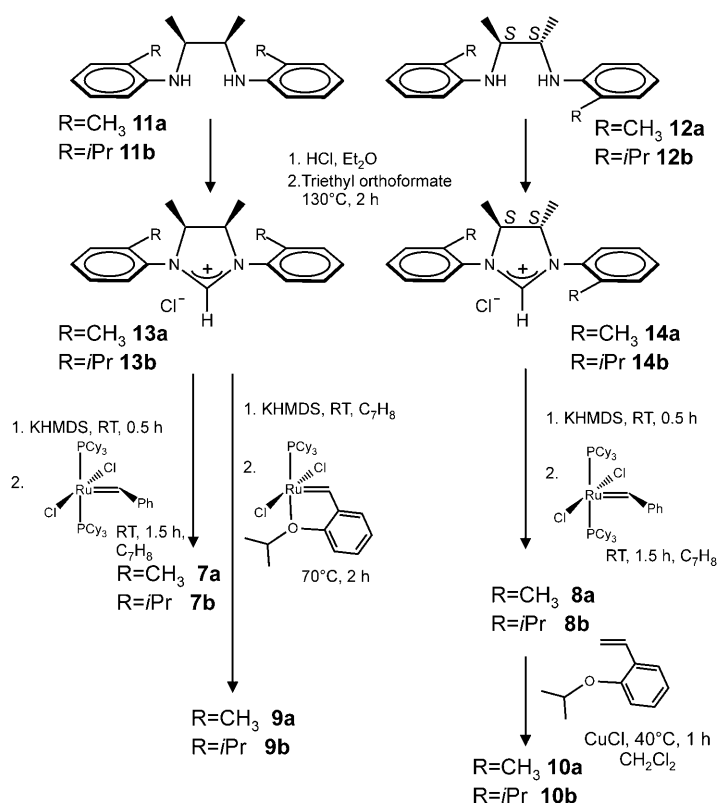


(**7a**) is the most active monophosphine catalyst known in the RCM of hindered olefins up to now.^[14] Since the different catalytic behaviors of *syn*- and *anti*-backbone-substituted NHC Ru complexes can stem from steric factors only, we reasoned that changing the bulkiness in the *ortho*-position of the N-substituent by replacing the Me group by an *i*Pr group (**7b** and **8b**) could have a (possibly) beneficial impact on RCM performances. We thus report here the synthesis and the catalytic performance of **7b** and **8b** in the RCM of differently substituted substrates. For a more comprehensive picture, we also present the synthesis, characterization and catalytic behavior of the corresponding phosphine-free precatalysts **9a**, **9b**, **10a** and **10b**.

Considering that the RCM of sterically encumbered olefins represents a challenging topic with a still incomplete mechanistic understanding, and that computational studies have contributed to remarkably increasing our knowledge of olefin metathesis,^[15–23] we decided to complement our experimental investigations with a complete DFT characterization of the entire RCM catalytic cycle, from substrate coordination to the release of the RCM products. This allowed us to better understand the different behaviors of NHC Ru catalysts bearing *syn*- and *anti*-methyl substituents on the backbone.

Results and Discussion

Synthesis and characterization of the complexes [RuCl₂(NHC)(=CHPh)(PCy₃)] and [RuCl₂(NHC)(=CH-*o*-*i*PrO-Ph)]: In order to study the effect of bulkier *N*-aryl groups on the reactivity of the related NHC ruthenium complexes bearing *syn*- and *anti*-methyl substituents on the backbone, we prepared phosphine-based complexes **7b** and **8b**, following synthetic protocols previously reported by our group (Scheme 1).^[14] Dihydromidazolium chlorides containing *N*-



Scheme 1. Synthesis of catalysts **7**–**10**.

o-isopropylphenyl groups (**13b** and **14b**) were obtained in high yields from cyclization of diamines **11b** and **12b** in the presence of HCl and triethyl orthoformate. The correspond-

ing free carbenes were generated in situ by treatment of these salts with potassium hexamethyldisilazide (KHMDs) in toluene at room temperature and were then treated with $[\text{RuCl}_2(=\text{CHPh})(\text{PCy}_3)_2]$ (Ph = phenyl, Cy = cyclohexyl, **1**) to afford the desired precatalysts **7b** and **8b**. Both complexes were isolated as air- and moisture-stable solids after flash column chromatography and were fully characterized by ^1H , ^{13}C , and ^{31}P NMR spectroscopy, which showed that at room temperature there is evidence for the presence of two isomers for both **7b** and **8b**, respectively. Any attempt to obtain crystalline material for X-ray diffraction studies failed.

To explore the catalytic potential of another important class of Ru-based olefin metathesis initiators, such as ether-based systems, we decided to undertake the synthesis of complexes **9a**, **9b**, **10a**, and **10b**, featuring our modified NHC ligands. As depicted in Scheme 1, imidazolium salts **13a** and **13b** were each treated with KHMDs and commercially available $[\text{RuCl}_2(=\text{CH}-o\text{-}i\text{PrO}-\text{Ph})(\text{PCy}_3)_2]$ in toluene at 70°C to afford the corresponding precatalysts **9a** and **9b**. To obtain complexes **10a** and **10b** in a satisfactory yields, we chose the alternative route that involves the reaction of Grubbs second-generation type complexes **8a** and **8b** with 2-isopropoxystyrene in the presence of CuCl at 40°C in CH_2Cl_2 (Scheme 1). The air- and moisture-stable complexes **10a** and **10b** were isolated as green microcrystalline solids after purification by column chromatography over silica gel. ^1H and ^{13}C NMR spectroscopic analyses of complexes **9a**, **9b**, **10a**, and **10b** revealed the existence of two isomers each. Single crystals suitable for X-ray structure analysis were obtained for **9a** and **9b** by vapor diffusion of pentane into concentrated benzene solutions of the precatalysts at room temperature.

ORTEP^[24] drawings of compounds **9a** and **9b** are shown in Figure 1. In both complexes, the Ru center is penta-coordinated and adopts a distorted square pyramidal coordination geometry. The two chlorine atoms are *trans* oriented in the basal plane of the square pyramid with the ether O atom and the imidazolyl C1 atoms, in mutual *trans* positions, occupying the remaining sites. The benzylidene ligand is situated in the apical position and is almost coplanar with the NHC ring, being rotated with respect to each other by only $18.28(1)$ and $19.5(1)^\circ$ in complexes **9a** and **9b**, respectively. In **9a**, the Ru atom is positioned 0.39 \AA above the basal plane toward the C20 carbene atom. The C6/C11 and C13/C18 phenyl rings are twisted with respect to the NHC ring by $78.24(1)$ and $69.1(2)^\circ$, respectively. These conformations are associated with the C–H $\cdots\pi$ ^[25] interaction between the C20–H20 group of the benzylidene moiety and the centroid C of the C6/C11 phenyl ring ($\text{H20}\cdots\text{C}(\text{C6}/\text{C11})=2.70 \text{ \AA}$, $\text{C20-H20}\cdots\text{C}=141^\circ$), and the C–H $\cdots\text{Cl}$ interaction^[26] between the C18–H18 moiety of the C13/C18 phenyl group and the Cl1 atom ($\text{H18}\cdots\text{Cl1}=2.78 \text{ \AA}$, $\text{C18-H18}\cdots\text{Cl1}=137^\circ$). In **9b**, the Ru atom is positioned 0.38 \AA above the basal plane toward the C24 carbene atom. The C6/C11 and C15/C20 phenyl rings are rotated with respect to the NHC ring by $84.7(1)$ and $65.5(1)^\circ$, respectively. Also in this structure,

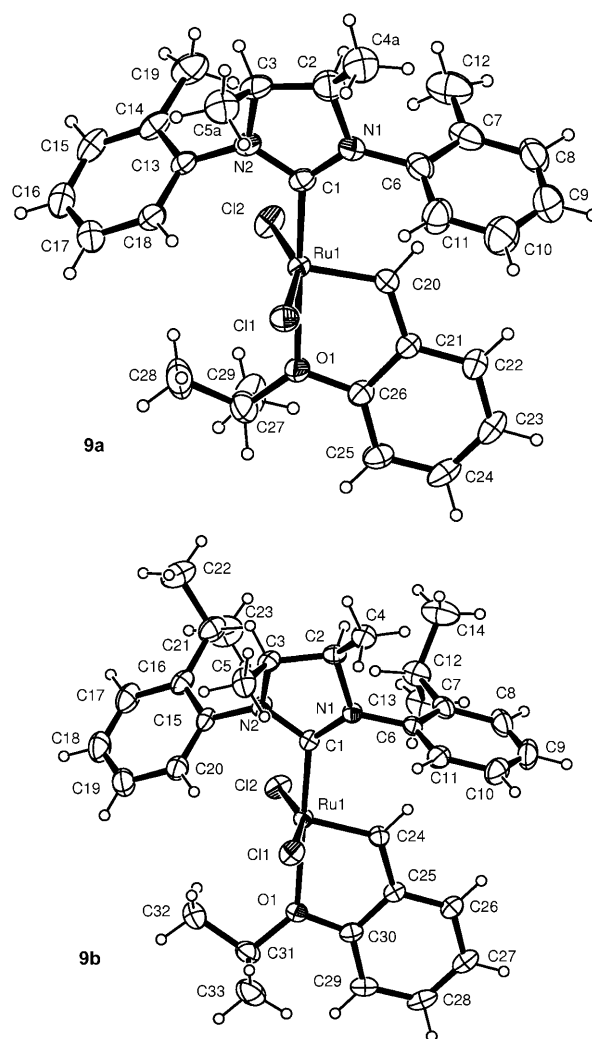


Figure 1. ORTEP^[24] drawings of complexes **9a** and **9b** with the thermal ellipsoids at 30% probability.

the analogous C24–H24 $\cdots\text{C}(\text{C6}/\text{C11})$ ($\text{H24}\cdots\text{C}=2.53 \text{ \AA}$, $\text{C24-H24}\cdots\text{C}=160^\circ$) and C20–H20 $\cdots\text{Cl1}$ ($\text{H20}\cdots\text{Cl1}=2.79 \text{ \AA}$, $\text{C20-H20}\cdots\text{Cl1}=147^\circ$) intramolecular interactions contribute in determining the conformations of the phenyl substituents at the NHC ring. All of the structural parameters for **9a** and **9b** are in good agreement with those observed for other complexes of the Hoveyda–Grubbs second-generation type that have been characterized crystallographically, regardless of the substituents on the NHC ring.^[6,10,11,27–34] Unfortunately, only polycrystalline agglomerates, not suitable for X-ray diffraction studies, could be obtained from complexes **10a** and **10b**.

RCM of selected substrates: The behaviors of the new phosphine-based complexes **7b** and **8b** and ether-based complexes **9a**, **9b**, **10a**, and **10b** were tested in the RCM of diethyl diallylmalonate **15** (Figure 2), diethyl allylmethylmalonate **17** (Figure 3), and diethyl dimethylmalonate **19** (Figure 4). The RCM reaction of each substrate was fol-

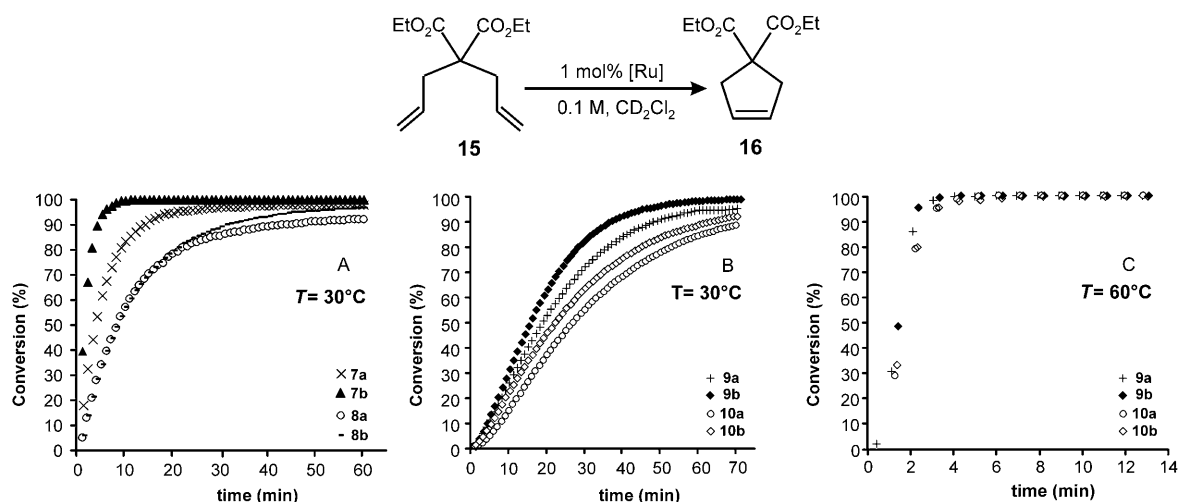


Figure 2. Kinetic plots of the RCM of **15**. Reaction conditions: A) and B) 1 mol% of catalyst, 30°C, 0.1 M substrate, CD₂Cl₂; C) 1 mol% catalyst, 60°C, 0.1 M substrate, C₆D₆.

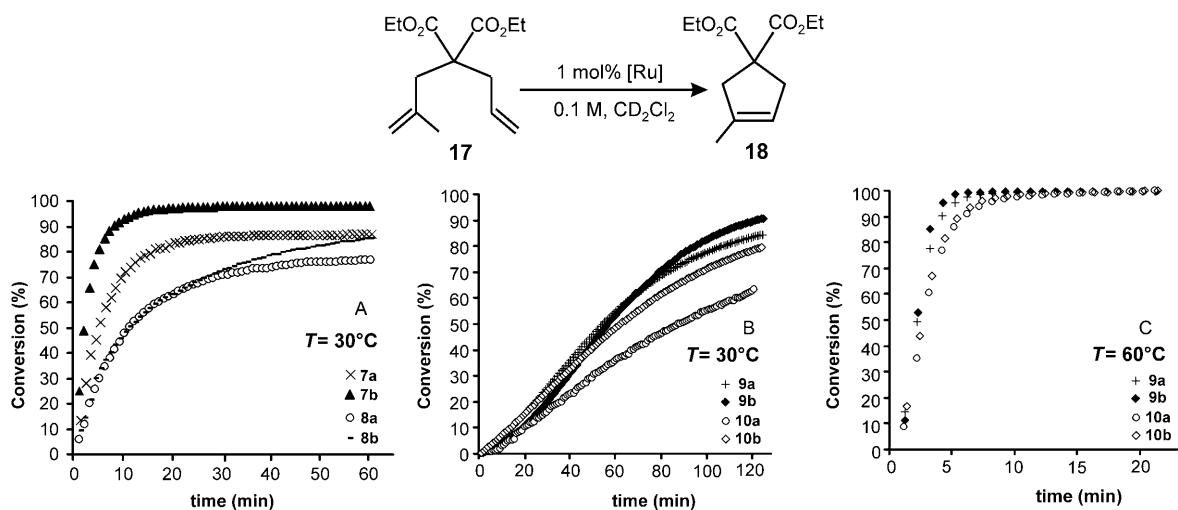


Figure 3. Kinetic plots of the RCM of **17**. Reaction conditions: A) and B) 1 mol% of catalyst, 30°C, 0.1 M substrate, CD₂Cl₂; C) 1 mol% catalyst, 60°C, 0.1 M substrate, C₆D₆.

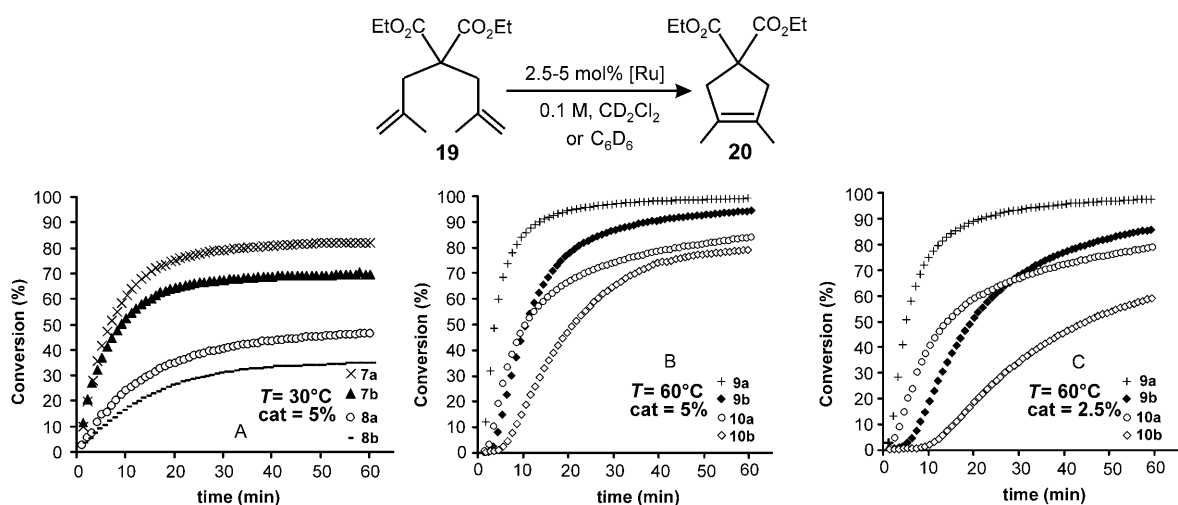


Figure 4. Kinetic plots of the RCM of **19**. Reaction conditions: A) 5 mol% of catalyst, 30°C, 0.1 M substrate, CD₂Cl₂; B) 5 mol% catalyst, 60°C, 0.1 M substrate, C₆D₆; C) 2.5 mol% catalyst, 60°C, 0.1 M substrate, C₆D₆.

lowed using ^1H NMR spectroscopy. For comparison, the plots of catalysts **7a** and **8a** are also shown.^[14]

The plots shown in Figure 2A indicate that the four mono-phosphine catalysts **7a**, **7b**, **8a** and **8b** are highly active in the RCM of **15**. Interestingly, the *syn* complexes **7a** and **7b** perform slightly better than the corresponding *anti* complexes **8a** and **8b**. The bulkier *syn* complex **7b** shows the highest initial reaction rate, reaching full conversion in 13 min, whereas the less bulky analogue **7a** needs more than 30 min to nearly complete the same transformation (>97% conversion). Conversely, the kinetic behaviors of the *anti* complexes **8a** and **8b** are very similar in the first 20 min (the initial reaction rate for **8a** and **8b** is the same). After 60 min, **8b** achieves slightly higher conversion (92% and >96% for **8a** and **8b**, respectively). Consistent with previous results,^[8,29,34] the slow to initiate phosphine-free complexes **9a**, **9b**, **10a**, and **10b** exhibit an overall lower catalytic activity under the same catalytic conditions (Figure 2B). The different reactivities presented by the two catalyst families could be related to their different mechanism of activation. In fact, while phosphine-containing catalysts initiate through a well-established dissociative mechanism,^[35,36] Hoveyda–Grubbs catalysts seems to initiate through an interchange mechanism, possibly with associative character.^[34,37] To promote activation of **9a**, **9b**, **10a**, and **10b**, the RCM of **15** was carried out at higher temperatures. At 60°C, the ether-based complexes are very efficient catalysts for the RCM of **15** (Figure 2C), reaching complete conversion within a few minutes. Once again, the *syn* complexes (**9a** and **9b** in this case) perform better than their *anti* analogues **10a** and **10b**.

The kinetic plots of the sterically more demanding RCM of diethyl allylmethylmalonate (**17**) are shown in Figure 3. Similar to the RCM of **15**, the *syn* complexes **7a** and **7b** show higher activity than the *anti* complexes **8a** and **8b** (Figure 3A). Once again, the bulkier *syn* complex **7b** turns out to be the most active catalyst (>95% conversion within 20 min), whereas the *syn* complex **7a** reaches a plateau at 85% conversion. It is important to underline that complex **7b** emerges among the most efficient NHC Ru-based catalysts for the RCM reaction of both **15** and **17**.^[38] The *anti* complexes **8a** and **8b** exhibit nearly identical profiles at the beginning of the reaction. Their behaviors differentiate at longer reaction times, which confirms a slightly higher activity (or higher stability) for the bulkier precatalyst **8b**. Under the same catalytic conditions, the phosphine-free catalysts **9a**, **9b**, **10a**, and **10b** are again visibly slower (Figure 3B). As in case of the RCM of **15**, increasing the temperature to 60°C allowed for quantitative cyclization of **17** in less than 20 min (Figure 3C).

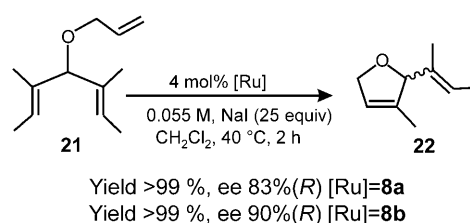
The results for the RCM of **19** to form the tetrasubstituted **20** ring, promoted by catalysts **7a**, **7b**, **8a**, and **8b** are shown in Figure 4A. With this sterically demanding substrate (**19**), the *syn* complexes exhibit higher conversions than the *anti* analogues. However, unlike with the RCM of **15** and **17**, in this case, the less bulky precatalysts **7a** and **8a** performed better than the more hindered congeners **7b** and

8b. Conversion of **19** was always incomplete and ranged between 35% (**8b**) and 82% (**7a**), the latter representing until now the best result achieved in this RCM reaction in the presence of monophosphine Ru catalysts. This minor efficiency is likely due to the high decomposition rate of the catalysts, clearly illustrated from the curvature in the logarithmic plot ($\ln(\text{starting material})$ versus time, see the Supporting Information). The very challenging RCM of **19** was also carried out with oxygen-chelated catalysts **9a**, **9b**, **10a**, and **10b** at 60°C to compensate for their slow initial rate.^[39] As depicted in Figure 4B, the four catalysts **9a**, **9b**, **10a**, and **10b** efficiently catalyze this ring closing, displaying the same reactivity trend observed for the corresponding phosphine-containing complexes. The differences in overall activity are much less pronounced than for phosphine-based complexes (Figure 4A), and conversions to the desired cyclized product **20** vary from good (63% for **10b**) to excellent (>95% for **9a**) within 30 min. The ring closure of **19** was successfully accomplished by decreasing the catalyst loading down to 2.5 mol% (Figure 4C), underlining the high efficiency of the *syn* complexes **9a** and **9b** in the RCM of hindered olefins. Remarkably, the less bulky *syn* precatalyst **9a** is the most effective, nearly completing the cyclization of **19** (>95%) in 40 min. Noteworthy is the fact that *syn*-**9b** and *anti*-**10b** complexes with bulkier *N*-aryl substituents on the NHC ligand show distinct differences in the initial reaction rates with respect to the less sterically encumbered *syn*-**9a** and *anti*-**10a** complexes (Figures 4B and 4C). This behavior seems to support an interchange mechanism, possibly with associative character, for the first step of the initiation reaction.^[37] Indeed, more sterically encumbered substrates would hardly be able to approach more sterically hindered complexes.

The above results suggest that 1) precatalysts with a *syn* orientation of the methyl groups on the NHC backbone are more active than their *anti* analogues and 2) bulky *N*-aryl groups, such as an *o*-isopropylphenyl ring, play an important role in improving catalytic performances in the RCM of **15** and **17**, whereas the challenging RCM of **19**, leading to a tetrasubstituted olefin, benefits from the reduced steric hindrance given by a *o*-tolyl ring. This indicates that *syn* and *anti* configurations of the NHC backbone, combined with *N*-substituents of different bulkiness, and to a different flexibility around the *N*-substituent bond, allow NHCs to modulate their encumbrance around the metal, providing differently shaped reactive pockets.^[21] According to these results, the challenging RCM of hindered olefins can be successfully accomplished by using: 1) Ru complexes with reduced *N*-aryl steric bulk on the NHC ligand;^[9,10] 2) Ru complexes bearing NHCs with restricted conformational freedom;^[11,14] 3) [(NHC)(NHC_{ewg})RuCl₂(CHPh)] (ewg = electron-withdrawing group) complexes;^[40] and 4) perfluorinated solvents.^[41,42] The first strategy allows for the design of reactive pockets large enough to accommodate sterically demanding tetrasubstituted olefins, while the second strategy restricts rotation around the *N*-aryl bond, preventing catalyst decomposition. Complexes **7**–**10** incorporate key elements of these two

ligand-design strategies. In fact, they are characterized by NHC ligands with substituents on the backbone and low but adaptable *N*-aryl bulk, which allows for the selection of the best catalyst to reach top performances in the RCM of unhindered as well as hindered substrates. Nevertheless, an emerging key element for the successful RCM of olefins derives from our findings: the symmetry of the NHC backbone plays a crucial role in activity of the Ru catalyst, which is amplified in the formation of tetrasubstituted olefins.

Asymmetric ring-closing metathesis (ARCM): The C_2 symmetric catalysts **8a** and **8b** were also tested in the ARCM of



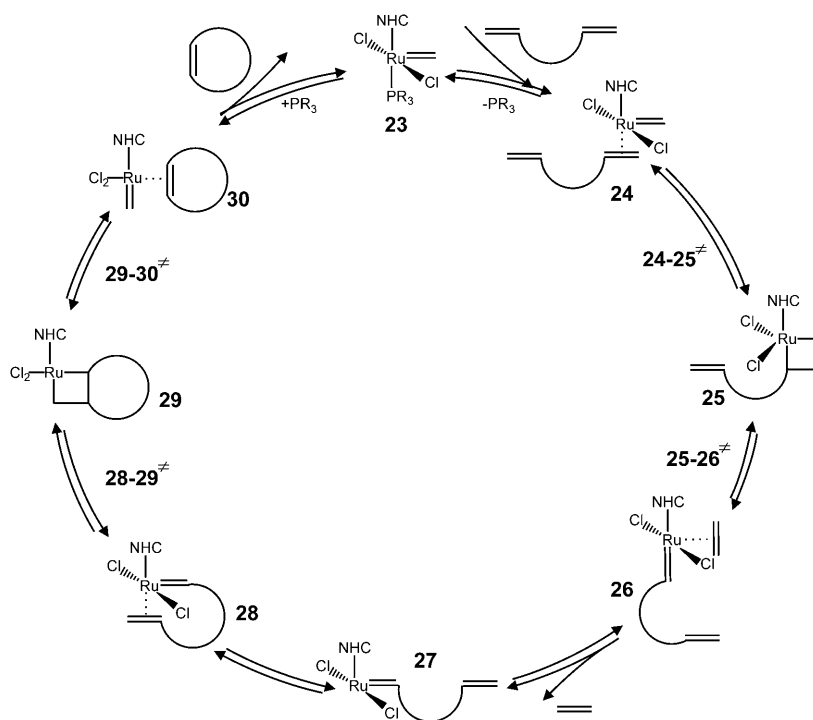
Scheme 2. ARCM of **21**.

a standard achiral substrate (**21**, Scheme 2).^[41] Both catalysts gave very high yields (>99%) and high *ee* values (83 and 90% for **8a** and **8b**, respectively). This performance is very similar to that exhibited by catalysts bearing *anti*-Ph substituents on the NHC backbone (*N*-*o*-tolyl substituents gave *ee* = 85%, while *N*-isopropylphenyl substituents gave *ee* = 90%).^[43] The consistency between our results and those found in the literature further supports the origin of enantioselectivity in the desymmetrization of achiral trienes, which is based on a chiral folding of the *N*-substituents induced by the substituents on the NHC backbone.^[16,21] This folding, confirmed by a NMR study,^[44] and dictated by steric interactions between the *ortho* substituents and the halides,^[21] forces the less bulky side of the *N*-substituent toward the substrate, so that the more bulky side of the *N*-substituent appears smaller to the substrate.^[44] In this context, the nature of the substituents on the NHC skeleton should have no major impact on stereoselectivity. Our findings that catalysts bearing Me substituents on the NHC backbone yield *ee* values that are very similar to those

for catalysts bearing Ph substituents, substantially confirm this scenario.

Molecular modeling studies: The experimental results reported in the previous section indicate that efficient RCM of **19** strongly depends on the *syn* or *anti* orientation of the methyl substituents on the NHC backbone, with *syn* catalysts **7a**, **7b**, **9a**, and **9b** leading to higher conversions with respect to their *anti* analogues **8a**, **8b**, **10a**, and **10b**. To rationalize this effect, the reaction pathway of the RCM of **19** (Scheme 3) was investigated computationally for catalysts **7a** and **8a**. Since the substrate coordinated species **24** is accepted to be in equilibrium with the phosphine coordinated species **23** during RCM,^[35,36,45] we assumed **23** to be the reference structure at zero free energy. The formation of the intermediates **24** and **28** (Scheme 3) can involve the coordination of both prochiral olefin faces. For the sake of clarity, from now on only the coordination of the prochiral olefin faces leading to minimum energy profiles will be discussed, although all possible structures are reported in the Supporting Information.

The free-energy profiles for the RCM of a model of **19** (in which the -COOEt group has been replaced by a -CH₃



Scheme 3. The general mechanism of the RCM of dienes.

group) with catalysts **7a** and **8a** are shown in Figure 5 (blue and red lines, respectively) together with the free-energy profile for the RCM of a model of **15** with catalyst **7a** (Figure 5, green lines). Comparison of the red and blue lines sheds light on the role of the *syn* or *anti* substitution on the NHC backbone, while comparison of the blue and green

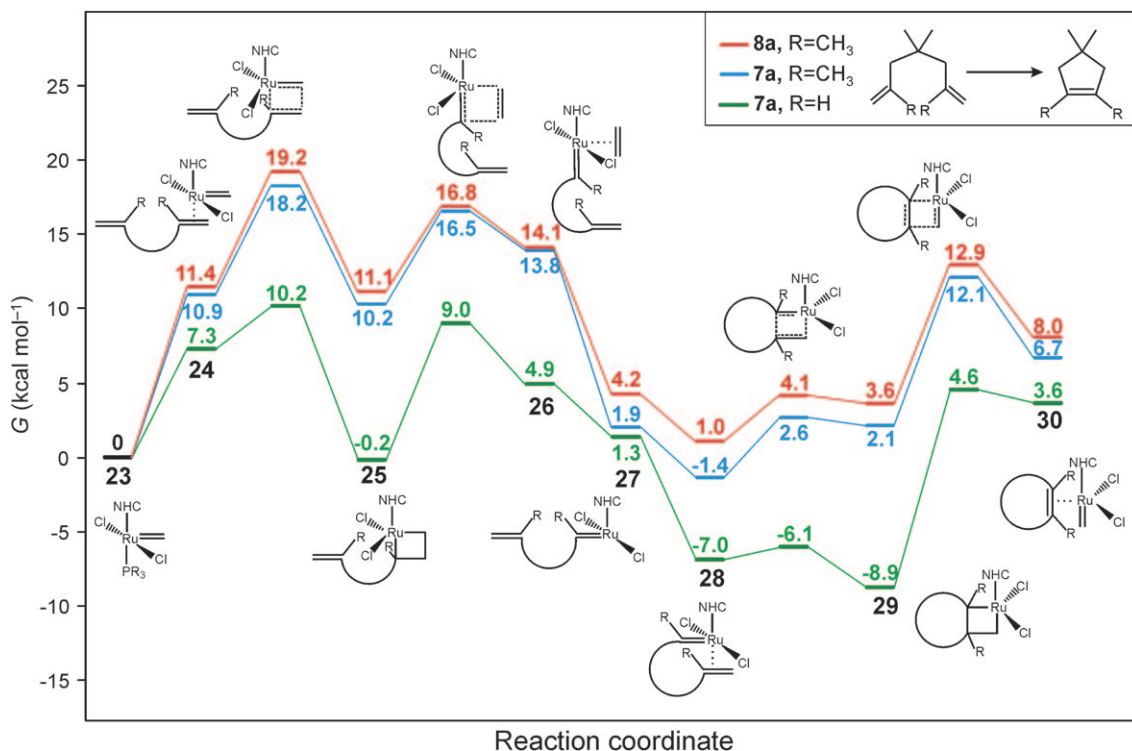


Figure 5. Free energy profiles of the RCM of a model of **19** in the presence of catalysts **7a** (blue) and **8a** (red) and of a model of **15** with catalyst **7a** (green).

lines sheds light on the role of the substrate substitution. The RCM profiles can be ideally split into three steps: 1) activation of the catalyst by substitution of PCy₃ with the substrate (**23** and **24**); 2) first metathesis between the substrate and the Ru–methylidene moiety (**24**–**26**); and 3) ring closing with product release (**27**–**30**). In line with experimental and theoretical results, PCy₃ substitution by the substrate, the pathway from **23** to **24**, is endergonic.^[15,35] As expected, the smaller substrate (green line, 7.3 kcal mol⁻¹) coordinates better than the bulkier one (blue line at 10.9 kcal mol⁻¹). It is, however, important that PCy₃ substitution by the substrate is favored by the *syn* catalyst (**7a**, by 0.5 kcal mol⁻¹) over the *anti* catalyst (**8a**, red line, 11.4 kcal mol⁻¹).

After the substrate has coordinated to the catalyst, the first metathesis step, through transition state **24**–**25**[‡], leads to the first metallacycle intermediate **25**. Visual inspection of Figure 5 clearly indicates that, regardless of the substrate or the catalyst, **24**–**25**[‡] is the transition state with the highest energy along the whole reaction pathway. The energy difference between transition state **24**–**25**[‡] and the starting complex **23** can be qualitatively related to the experimental RCM activity and, in line with the kinetic experiments, the transition state **24**–**25**[‡] for the smaller substrate (green line, 10.2 kcal mol⁻¹) is quite lower in energy relative to the corresponding transition states for the bulkier substrate, both with the *syn* and *anti* catalysts **7a** and **8a** (blue and red lines, 18.2 and 19.2 kcal mol⁻¹, respectively). Focusing on the bulkier substrate, the small energy preference (1.0 kcal mol⁻¹) for the transition state **24**–**25**[‡] with the *syn* catalyst

7a also is in qualitative agreement with the faster kinetics of the RCM of **19** with **7a** than with **8a** (Figure 4). The transition state **24**–**25**[‡] collapses into metallacycle **25** that, in agreement with experimental evidence,^[45] is a rather stable free-energy sink along the reaction pathway.

After metallacycle **25** has been reached, the reaction proceeds through a series of well-accepted steps. Ring opening through the transition state **25**–**26**[‡] leads to the ethylene coordination intermediate **26**, from which ethylene is released. Ethylene dissociation from the catalyst, favored by entropic factors, leads to the 14e intermediate **27**, followed by coordination of the second C=C bond of the substrate, giving coordination intermediate **28**. Also in this coordination intermediate, the smaller substrate coordinates better than the bulkier substrate on the *syn* catalyst (Figure 5, green and blue lines, -7.0 and -1.4 kcal mol⁻¹, respectively), and coordination of the bulkier substrate to the *syn* catalyst is slightly favored over coordination to the *anti* catalyst (red line, 1.0 kcal mol⁻¹). The ring-closing step proceeds through the transition state **28**–**29**[‡], which collapses into metallacycle **29**. Interestingly, in case of the smaller substrate metallacycle **29** is slightly preferred over the coordination intermediate **28**, whereas, in case of the bulkier substrate, the metallacycle is higher in energy. In agreement with the experimental results,^[46] this indicates that the stability of the metallacycle relative to the coordination intermediate is reduced by the formation of a five-membered ring and also depends on the bulkiness of the substrate. The product release step, through transition state **29**–**30**[‡], leads to the product coordinated in-

intermediate **30**, from which, with the hypothesis that another substrate is able to trap the active species before PCy₃ coordination, another RCM reaction can start. Since the ring-closing step transforming **28** to **30** is much lower in energy relative to the rate-determining reaction of **23** to **25**, we will not go into further detail. We will only remark that, in agreement with experimental results,^[45] the product formation transition state **29-30**[‡] is much higher in energy relative to the ring-closing transition state **28-29**[‡], which we believe further supports the validity of the shape of the free-energy profile we computed. However, because the differences between the various systems stem from transition state **24-25**[‡], we will focus our analysis on this point.

The transition states **24-25**[‡] for the bulkier substrate, both with **7a** and **8a**, are shown in Figure 6. The main differ-

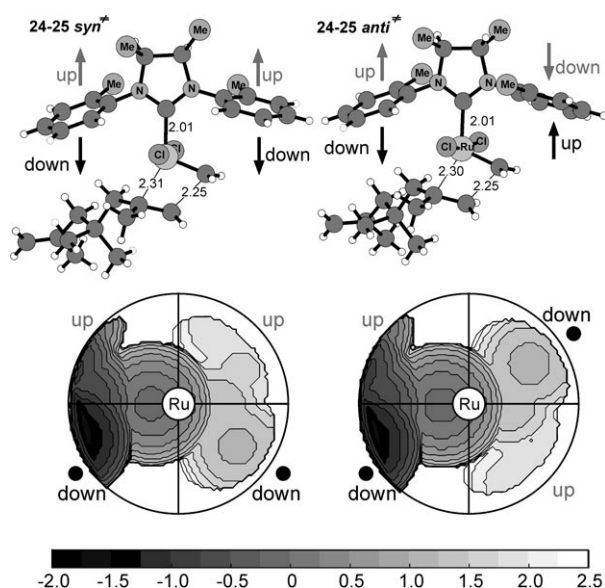


Figure 6. Top) Geometries of the transition state **24-25**[‡] for both the *syn* catalyst **7a** and the *anti* catalyst **8a**. Distances are given in Å. Bottom) The corresponding steric maps of the NHC ligands. The quadrants corresponding to the unsubstituted side of the *o*-tolyl rings is indicated by a black spot. Values of the isocontour lines are given in Å. In the quadrants representation, the systems are viewed along the NHC–Ru bond.

ence between the two structures is in the relative disposition of the unsubstituted side of the *o*-tolyl rings, which are consistently folded down (i.e. towards the substrate).^[16,21,44] In the structure of the *syn* catalyst **7a**, the rings are on the same side of the NHC plane, and thus the two *o*-tolyl rings make a substantially flat reactive pocket characterized by a glide plane. Conversely, in the *anti* catalyst **8a**, the rings are on opposite sides of the NHC plane, and thus the two *o*-tolyl rings form a reactive pocket acting like a wrench, squeezing the substrate and the Ru–alkylidene bond.

These features are best appreciated by looking at the steric maps of the NHC ligands in the transition state **24-25**[‡] (Figure 6). The steric map of **7a** shows that steric pressure from the *o*-tolyl rings is indeed in the bottom two quadrants, and that there is more space available in the two top

quadrants, while in case of **8a**, steric pressure is in the bottom-left and top-right quadrants. The differently shaped reactive pockets result in very different interactions around the methylidene moiety and the *o*-tolyl ring. In the *anti* transition state **24-25**[‡] these two groups are rotated with respect to one another by roughly 16°, which results in the C_{ortho} on the unsubstituted side of the *o*-tolyl ring and the nearby H_{methylidene} at a distance of only 3.0 Å (Figure 7). Conversely,

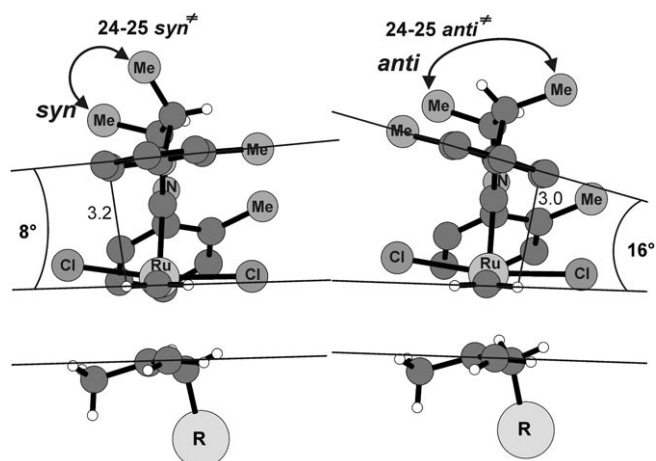


Figure 7. Side view of the transition state **24-25**[‡] for the *syn* catalyst **7a** and the *anti* catalyst **8a**. Distances are given in Å.

in the *syn* transition state **24-25**[‡] the interaction between these two groups is more relaxed because the angle between the two planes is minor (only 8°), which results in the C_{ortho} on the unsubstituted side of the *o*-tolyl ring and the nearby H_{methylidene} at a distance of 3.2 Å (Figure 7). In other words, the geometry of the reacting atoms can better follow the flat shape casted by the *syn* catalyst, rather than the zig-zag shape of the *anti* catalyst. The side view of the transition states **24-25**[‡] (Figure 7) also shows the relative orientation of the main plane of the *o*-tolyl ring and of the alkylidene moiety, indicating that, in the *anti* catalyst, these two planes are rotated in opposite directions, resulting in the C_{ortho}–H_{methylidene} steric clash described above.

Finally, to exclude that the different reactivity of **7a** and **8a** is related to a different ratio in the number of productive/non productive metathesis events,^[47] we also located transition state **24-25-NP**[‡] (nonproductive metathesis), in which the substrate reacts as shown in Figure 8. These two transition states are at 15.0 and 15.4 kcal mol⁻¹ above **23**+ free substrate for **7a** and **8a**, respectively, which indicates that, for both the *syn* and *anti* catalysts, nonproductive metathesis is largely favored over productive metathesis by roughly 3–4 kcal mol⁻¹. More relevant to the present work, however, is the fact that, in case of nonproductive metathesis, the *syn*-**24-25-NP**[‡] transition state is favored over the *anti*-**24-25-NP**[‡] transition state, which means that the minor reactivity of the *anti* catalyst cannot be connected to a higher propensity of the *anti* catalyst to nonproductive metathesis.

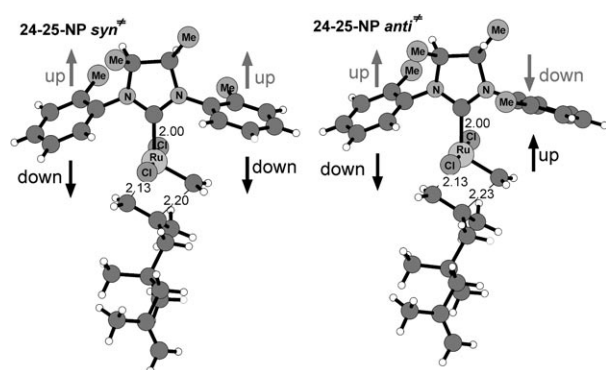


Figure 8. Geometries of the transition state **24-25-NP[‡]** for both the *syn* catalyst **7a** and the *anti* catalyst **8a**. Distances are given in Å.

Kinetic initiation studies: Activation parameters for the initiation reaction of catalysts **7a** and **8a** were determined by reacting these complexes with butyl vinyl ether. It is generally accepted that this reaction is irreversible, giving inactive metathesis species.^[34–36,48] Reactions were conducted at four different temperatures, and the parameters (Table 1) were

Table 1. Activation parameters for the initiation of catalysts **7a** and **8a**.

Catalyst	ΔH^\ddagger [kcal mol ⁻¹]	ΔS^\ddagger [cal mol ⁻¹ K ⁻¹]	ΔG^\ddagger (298 K) [kcal mol ⁻¹]
7a	30 ± 2	+26 ± 7	21.86 ± 0.02
8a	31 ± 1	+28 ± 4	22.322 ± 0.009

extrapolated from the corresponding Eyring plots (see Supporting Information). The values for ΔG^\ddagger at 298 K are 21.86 and 22.32 kcal mol⁻¹ for **7a** and **8a**, respectively. The slight difference (0.46 kcal mol⁻¹) in the free-energy activation once again underlines that catalyst symmetry plays an important role in the very beginning of the reaction. It is worth noting that this $\Delta\Delta G^\ddagger$ is lower but comparable to the calculated $\Delta\Delta G^\ddagger$ between *syn*- and *anti*-**24-25[‡]** in the RCM of **19** (1.0 kcal mol⁻¹, Figure 5). Indeed, the initiation free-energy barrier gap could be amplified by the presence of sterically hindered olefins. This statement is supported by the experimental observation that the activity difference between **7a** and **8a** increases by increasing the substrate hindrance (Figures 2 A, 3 A, and 4 A).

Conclusion

Here, we report the synthesis and characterization of new Ru-based catalysts, containing N-heterocyclic carbene ligands with *syn* and *anti* orientation of the methyl groups on the NHC backbone and aryl N-substituents of different

bulkiness (*o*-tolyl or *o*-isopropylphenyl). The catalytic behavior of the phosphine-containing ruthenium complexes **7** and **8** and of the ether-based complexes **9** and **10** in the RCM of diethyl diallylmalonate (**15**), diethyl allylmethylmalonate (**17**), and diethyl dimethylmalonate (**19**) was investigated. These complexes are highly efficient catalysts for RCM reactions. Furthermore, the catalysts with a *syn* orientation of the methyl groups on the NHC backbone performed better than their *anti* analogues. In particular, the *syn* complexes with *o*-tolyl N-substituents (**7a** and **9a**) are among the most efficient catalysts in the formation of tetra-substituted olefins. The beneficial effect of the *syn* backbone is clearly noticeable in both phosphine and phosphine-free catalysts, highlighting that the observed reactivity is independent of the initiation mechanism. This finding makes the NHC backbone symmetry a new key element that needs to be taken into account in designing ruthenium catalysts for olefin metathesis.

The pivotal role of the *syn* and *anti* orientations of the methyl groups on the NHC backbone in the catalyst activity was rationalized by investigating the RCM of a sterically hindered olefin (**19**) with catalysts **7a** and **8a** and through DFT calculations. To the best of our knowledge, this is the first time that the entire RCM catalytic cycle was investigated for hindered olefins by theoretical studies. Free energy profiles of the RCM showed that the rate-determining step of the reaction is located at the very beginning of the catalytic cycle. According to our calculations, the activity difference between **7a** and **8a** is determined by the different energy barrier of the first cross metathesis of one of the substrate double bonds. The marked drop in the free-energy barrier for this step, in the case of a much less sterically encumbered olefin **15**, supports this interpretation and rationalizes the higher activity of those catalysts toward less hindered substrates. The location of the rate-determining step at the very beginning of the reaction was further confirmed by kinetic initiation studies performed on **7a** and **8a**. In fact, ΔG^\ddagger was shown to be slightly lower in the presence of the catalyst bearing *syn*-methyl groups on the NHC backbone (**7a**).

Experimental Section

General information: All of the reactions were carried out using standard Schlenk or glovebox techniques under nitrogen. All of the reagents were purchased from Sigma-Aldrich and were of reagent grade quality. These reagents were used as received. The solvents were dried and distilled before use. Deuterated solvents were degassed under a nitrogen flow and stored over activated 4 Å molecular sieves. Flash column chromatography of the organic compounds was performed using silica gel 60 (230–400 mesh), and flash column chromatography of the ruthenium compounds was performed using silica gel 60 (230–400 mesh) from TSI Scientific (Cambridge, MA). Analytical thin-layer chromatography (TLC) was performed using silica gel 60 F254 precoated plates (0.25 mm thickness) with a fluorescent indicator. Visualization of TLC plates was performed by UV light and KMnO₄ or I₂ stains. Enantiomeric excesses were determined by chiral GC (Chiraldex G-TA, 30 m × 0.25 mm) and were compared to racemic pure samples. NMR spectra were recorded on a Bruker

AM300 and a Bruker AVANCE 400 operating at 300 and 400 MHz for ^1H , respectively. The ^1H and ^{13}C NMR chemical shifts are referenced to SiMe_4 ($\delta = 0$ ppm) using the residual proton impurities of the deuterated solvents as internal standards. ^{31}P NMR spectra were referenced using H_3PO_4 ($\delta = 0$ ppm) as an external standard. Spectra are reported as follows: chemical shift (ppm), multiplicity, coupling constant (Hz), and integration. Multiplicities are abbreviated as follows: singlet (s), doublet (d), triplet (t), quartet (q), multiplet (m), and broad (br). Elemental analysis was done on a PERKIN-Elmer 240-C analyzer. Compounds **17**, **19**^[49], and **21**^[43], as well as ruthenium complexes **7a** and **8a**^[44] were prepared according to literature procedures.

[(*meso*)-1,3-Bis(2-isopropylphenyl)-4,5-dimethylimidazolin-2-ylidene]dichloro(benzylidene)(tricyclohexylphosphine)ruthenium(II) (7b): In a glovebox, a 50 mL Schlenk tube was charged with the imidazolium salt **13b** (0.77 mmol, 287 mg), potassium hexamethyldisilazide (KHMDs, 0.8 mmol, 159 mg), and toluene (6.9 mL). The reaction mixture was stirred at room temperature for 30 min. Then $[\text{Ru}(\text{PCy}_3)_2](=\text{CHPh})\text{Cl}_2$ (0.65 mmol, 538 mg) was added, and the reaction mixture was stirred for 1.5 h at room temperature. After this time, the reaction mixture was concentrated and purified by flash column silica gel chromatography (diethyl ether and pentane, 1:9 to 1:1) to afford **7b** as a green-brown powder (0.46 mmol, 405 mg, 60%). ^1H NMR (400 MHz, CD_2Cl_2): $\delta = 19.2$ (minor isomer: s, $\text{Ru}=\text{CHPh}$), 19.0 (major isomer: s, $\text{Ru}=\text{CHPh}$), 8.56 (d), 8.40 (d) 7.63–7.27 (m), 7.22–6.91 (m), 6.85–6.69 (m), 6.39 (brs), 4.70–4.37 (m), 4.23–4.03 (m), 3.67 (brs), 3.55 (s), 2.0–0.71 ppm (several peaks); ^{13}C NMR (100 MHz, C_6D_6): $\delta = 300.6$ (brs, $\text{Ru}=\text{CHPh}$), 219.6 (d, $J(\text{P},\text{C}) = 77.7$ Hz, $i\text{NCN}$), 217.6 (d, $J(\text{P},\text{C}) = 80.2$ Hz, $i\text{NCN}$), 152.1, 151.6, 149.1, 148.9, 148.7, 148.3, 148.2, 147, 138.8, 138.6, 138.2, 137.4, 137.1, 136.8, 136.2, 134.7, 134.2, 133.9, 133.7, 133.2, 131.1, 130.1, 129.8, 129.5, 129.2, 127.5, 127.4, 127.3, 127.2, 127, 126.8, 126.6, 126.3, 126.2, 65.9, 64.3, 63.4, 63.1, 62.8, 33.6, 33.5, 33.3, 33.2, 29.4, 29.2, 28.5, 28.4, 27.1, 27, 26.2, 25.9, 25.5, 24.9, 24.5, 14.2, 14, 13.8, 13.2, 12.9 ppm. ^{31}P NMR (161.97 MHz, C_6D_6): $\delta = 23.8$ (minor isomer) 22.6 ppm (major isomer); elemental analysis calcd (%) for $\text{C}_{48}\text{H}_{60}\text{Cl}_2\text{N}_2\text{PRu}$ (877.02): C 65.74, H 7.93, N 3.19; found C 65.70, H 7.96, N 3.20.

[(4*S*,5*S*)-1,3-Bis(2-isopropylphenyl)-4,5-dimethylimidazolin-2-ylidene]dichloro(benzylidene)(tricyclohexylphosphine)ruthenium(II) (8b): Using the procedure described for the preparation of **7b**, the imidazolium salt **14b** (0.90 mmol, 337 mg), KHMDs (0.94 mmol, 188 mg), and $[\text{Ru}(\text{PCy}_3)_2](=\text{CHPh})\text{Cl}_2$ (0.76 mmol, 629 mg) were reacted in toluene (8.1 mL), affording **8b** (0.58 mmol, 510 mg) in 65% yield as a brown powder (diethyl ether and pentane, 1:9 to 1:1). ^1H NMR (400 MHz, CD_2Cl_2): $\delta = 19.2$ (major isomer: s, $\text{Ru}=\text{CHPh}$), 19.1 (minor isomer: s, $\text{Ru}=\text{CHPh}$), 8.48 (d), 7.50–7.24 (m), 7.11–7.01 (m), 6.93 (brs), 6.82 (brt), 3.87 (m), 3.73 (m), 3.58 (m), 3.36 (brs), 1.84 (brm), 1.63–0.80 ppm (several peaks). ^{13}C NMR (100 MHz, C_6D_6): $\delta = 297.1$ (s, $\text{Ru}=\text{CHPh}$), 218.9 (d, $J(\text{P},\text{C}) = 76.8$ Hz, $i\text{NCN}$), 152, 149.2, 147.6, 137.5, 136.2, 135.8, 133.9, 132.5, 130.2, 127, 126.1, 68.2, 67.8, 33.5, 33.4, 30.5, 28.5, 27.8, 27.1, 26, 25.9, 24.7, 24.3, 20, 19.8 ppm; ^{31}P NMR (161.97 MHz, C_6D_6): $\delta = 24.9$ (major isomer), 22.3 ppm (minor isomer); elemental analysis calcd (%) for $\text{C}_{48}\text{H}_{60}\text{Cl}_2\text{N}_2\text{PRu}$ (877.02): C 65.74, H 7.93, N 3.19; found C 65.72, H 7.90, N 3.18.

[(*meso*)-1,3-Bis(2-methylphenyl)-4,5-dimethylimidazolin-2-ylidene]dichloro(2-isopropoxybenzylidene)ruthenium(II) (9a): In a glovebox, the imidazolium salt **13a**^[44] (0.47 mmol, 147 mg) and toluene (2 mL) were placed in a 50 mL Schlenk tube and stirred. KHMDs (0.51 mmol, 103 mg) was then added. The resulting solution was stirred at room temperature for ten minutes. $[\text{RuCl}_2(\text{PCy}_3)_2](=\text{CH-}o\text{-OiPrC}_6\text{H}_4)$ (0.25 mmol, 147 mg) was then added, and the mixture was stirred for 2 h at 70 °C. After cooling to room temperature, the mixture was purified by column chromatography on TSI silica gel (hexane and diethyl ether, 2:1 to 1:1) to give **9a** (0.15 mmol, 88 mg, 60%) as a green crystalline solid. ^1H NMR (400 MHz, CD_2Cl_2): $\delta = 16.34$ (major isomer: s, $\text{Ru}=\text{CH-}o\text{-OiPrC}_6\text{H}_4$), 16.26 (minor isomer: s, $\text{Ru}=\text{CH-}o\text{-OiPrC}_6\text{H}_4$), 8.59 (br d), 7.71–7.13 (m), 7.04 (brm), 6.92–6.68 (m), 4.96 (m), 4.73 (m), 4.53 (m), 4.32 (m), 4.07 (brs), 2.65 (d), 2.51 (d), 2.38 (d), 1.57–1.29 (m), 1.27–1.24 (m), 1.20–1.12 ppm (m); ^{13}C NMR (100 MHz, CD_2Cl_2): $\delta = 297.1$ (minor isomer), 295.5 (major isomer), 212.9, 209.3, 153.0, 152.7, 144.8, 144.5, 141.7, 140.5,

140.2, 140.0, 139.2, 138.9, 138.4, 131.1, 130.2, 130.0, 129.3, 129.1, 129, 128.3, 128, 127.6, 127.5, 126.9, 123, 122.7, 122.3, 113.5, 75.3, 66.0, 62.0, 61.4, 56.1, 36.1, 35.5, 30.6, 30.2, 28.3, 27.5, 27.4, 27.0, 26.8, 22.4, 22.2, 22.0, 19.5, 19.0, 18.5, 14.0, 13.8, 12.1 ppm; elemental analysis calcd (%) for $\text{C}_{29}\text{H}_{34}\text{Cl}_2\text{N}_2\text{ORu}$ (598.57): C 58.19, H 5.73, N 4.68; found C 58.20, H 5.70, N 4.68.

[(*meso*)-1,3-Bis(2-isopropylphenyl)-4,5-dimethylimidazolin-2-ylidene]dichloro(2-isopropoxybenzylidene)ruthenium(II) (9b): Using the procedure described for the preparation of **9a**, the reaction of the imidazolium salt **13b** (0.84 mmol, 312 mg), KHMDs (0.93 mmol, 184 mg) and $[\text{RuCl}_2(\text{PCy}_3)_2](=\text{CH-}o\text{-OiPrC}_6\text{H}_4)$ (0.45 mmol, 267 mg) in toluene (4 mL) afforded the desired compound **9b** (0.30 mmol, 200 mg) in 68% yield as a bright green crystalline solid (hexane and diethyl ether, 2:1 to 1:1). ^1H NMR (400 MHz, CD_2Cl_2): $\delta = 16.40$ (major isomer: s, $\text{Ru}=\text{CH-}o\text{-OiPrC}_6\text{H}_4$), 16.13 (minor isomer: s, $\text{Ru}=\text{CH-}o\text{-OiPrC}_6\text{H}_4$), 8.76 (d), 7.63–7.37 (m), 7.19 (t), 6.92–6.84 (m), 4.96 (m), 4.80 (m), 4.60 (m), 4.46 (m), 4.27 (m), 3.50 (m), 3.39–3.29 (m), 1.54–1.10 (overlapped peaks), 0.84 ppm (d); ^{13}C NMR (400 MHz, CD_2Cl_2): $\delta = 296.1$, 295.2, 209.9, 152.9, 148.7, 148.4, 148.2, 144.2, 140.6, 139.0, 138.6, 138.0, 132.3, 131.6, 130.1, 129.9, 129.6, 129.1, 128.7, 128.1, 127.9, 127.7, 122.8, 122.4, 122.1, 113.4, 75.1, 75.0, 66.5, 64.0, 63.3, 63.0, 28.9, 28.6, 28.5, 27.4, 25.9, 25.2, 25.0, 24.2, 24.1, 23.4, 23.2, 22.5, 22.1, 21.8, 14.1, 13.7, 12.7 ppm; elemental analysis calcd (%) for $\text{C}_{33}\text{H}_{42}\text{Cl}_2\text{N}_2\text{ORu}$ (654.67): C 60.54, H 6.47, N 4.28; found C 60.54, H 6.43, N 4.31.

[(4*S*,5*S*)-1,3-Bis(2-methylphenyl)-4,5-dimethylimidazolin-2-ylidene]dichloro(2-isopropoxybenzylidene)ruthenium(II) (10a): The ruthenium complex **8a**^[44] (0.15 mmol, 125 mg) and CuCl (0.17 mmol, 17 mg) were added to a 50 mL round bottom flask in a glovebox and were dissolved in dichloromethane (6 mL). A solution of 2-isopropoxystyrene (0.15 mmol, 25 mg) in CH_2Cl_2 (4 mL) was then added, and the resulting solution was stirred at 40 °C for 1 h. After cooling to room temperature, the solvent was removed in vacuo and the crude catalyst was purified by column chromatography (pentane and CH_2Cl_2 , 1:1) to afford **10a** as a green powder (0.11 mmol, 64 mg, 70%). ^1H NMR (300 MHz, CD_2Cl_2): $\delta = 16.57$ (brs, $\text{Ru}=\text{CH-}o\text{-OiPrC}_6\text{H}_4$), 16.42 (brs, $\text{Ru}=\text{CH-}o\text{-OiPrC}_6\text{H}_4$), 8.47 (brs), 7.57–7.39 (m), 6.91 (m), 4.91 (m), 4.20 (m), 4.00 (m), 2.49 (m), 1.90–1.71 (m), 1.35–1.26 ppm (m); ^{13}C NMR (75 MHz, CD_2Cl_2): $\delta = 296.7$, 295.6, 210.0, 152.6, 144.6, 141.4, 140.0, 139.1, 138.9, 138.2, 133.8, 132.9, 131.7, 131.6, 131.1, 130.3, 129.9, 129.2, 128.0, 127.2, 127.0, 122.7, 122.3, 113.3, 77.0, 75.2, 71.2, 66.9, 65.5, 64.7, 32.1, 31.7, 31.2, 29.1, 30.0, 29.7, 27.7, 27.5, 26.4, 25.6, 22.8, 19.9, 19.4, 18.8, 18.2 ppm; elemental analysis calcd (%) for $\text{C}_{29}\text{H}_{34}\text{Cl}_2\text{N}_2\text{ORu}$ (598.57): C 58.19, H 5.73, N 4.68; found C 58.20, H 5.70, N 4.68.

[(4*S*,5*S*)-1,3-Bis(2-isopropylphenyl)-4,5-dimethylimidazolin-2-ylidene]dichloro(2-isopropoxybenzylidene)ruthenium(II) (10b): Using the procedure reported for the synthesis of **10a**, the ruthenium complex **8b** (0.14 mmol, 120 mg), CuCl (0.15 mmol, 15 mg) and 2-isopropoxystyrene (0.14 mmol, 23 mg) were reacted in dichloromethane (10 mL) to give **10b** (0.12 mmol, 79 mg, 88%) as a green powder (hexane and CH_2Cl_2 , 1:1). ^1H NMR (300 MHz, CD_2Cl_2): $\delta = 16.36$ (s, $\text{Ru}=\text{CH-}o\text{-OiPrC}_6\text{H}_4$), 16.31 (s, $\text{Ru}=\text{CH-}o\text{-OiPrC}_6\text{H}_4$), 8.56 (d), 7.61–7.36 (m), 6.88 (m), 4.91 (m), 4.24 (m), 3.95 (m), 3.46 (m), 3.22 (m), 1.45–1.32 (m), 1.27 (m), 1.06 (m), 0.88 ppm (brm); ^{13}C NMR (75 MHz, CD_2Cl_2): $\delta = 296.3$, 295.6, 212.2, 209.9, 152.7, 149.9, 149.3, 149.1, 148.9, 144.6, 144.4, 140.4, 138.6, 137.1, 136.3, 134.2, 133.4, 132.9, 130.4, 129.8, 129.7, 129.6, 128.7, 127.7, 127.5, 126.4, 127.2, 127.0, 126.6, 122.8, 122.3, 122.1, 113.3, 75.2, 75.1, 71.2, 68.4, 67.1, 66.2, 30.4, 30.1, 29.8, 29.1, 28.6, 28.3, 28.0, 27.5, 26.3, 26.0, 25.6, 24.6, 24.2, 23.7, 23.0, 22.2, 22.0, 19.9 ppm; elemental analysis calcd (%) for $\text{C}_{33}\text{H}_{42}\text{Cl}_2\text{N}_2\text{ORu}$ (654.67): C 60.54, H 6.47, N 4.28; found C 60.54, H 6.43, N 4.31.

Acknowledgements

The authors thank Francesco Funicello for the helpful discussion and Patrizia Oliva for the technical assistance. LC gratefully acknowledges the EC for funding this work through the European Community's Sev-

ent Framework Programme (FP7/2007-2013) under grant agreement n°CP-FP 211468-2 EUMET. Computational support from CINECA - High Performance Computing Portal and financial support from the Ministero dell'Università e della Ricerca Scientifica e Tecnologica are gratefully acknowledged.

- [1] For selected reviews, see: a) A. Fürstner, *Angew. Chem.* **2000**, *112*, 3140–3172; *Angew. Chem. Int. Ed.* **2000**, *39*, 3012–3043; b) M. R. Buchmeiser, *Chem. Rev.* **2000**, *100*, 1565–1604; c) T. M. Trnka, R. H. Grubbs, *Acc. Chem. Res.* **2001**, *34*, 18–29; d) R. H. Grubbs, *Handbook of Metathesis*, Wiley-VCH, Weinheim, **2003**; e) R. R. Schrock, A. H. Hoveyda, *Angew. Chem.* **2003**, *115*, 4740–4782; *Angew. Chem. Int. Ed.* **2003**, *42*, 4592–4633; f) R. H. Grubbs, *Tetrahedron* **2004**, *60*, 7117–7140; g) D. Astruc, *New J. Chem.* **2005**, *29*, 42–56; h) K. C. Nicolaou, P. G. Bulger, D. Sarlah, *Angew. Chem.* **2005**, *117*, 4564–4601; *Angew. Chem. Int. Ed.* **2005**, *44*, 4490–4527; i) R. R. Schrock, *Angew. Chem.* **2006**, *118*, 3832–3844; *Angew. Chem. Int. Ed.* **2006**, *45*, 3748–3759; j) R. H. Grubbs, *Angew. Chem.* **2006**, *118*, 3845–3850; *Angew. Chem. Int. Ed.* **2006**, *45*, 3760–3765; k) A. H. Hoveyda, A. R. Zhugralin, *Nature* **2007**, *450*, 243–251; l) W. A. van Otterlo, C. B. de Koning, *Chem. Rev.* **2009**, *109*, 3743–3782.
- [2] a) P. H. Deshmukh, S. Blechert, *Dalton Trans.* **2007**, 2479–2491; b) C. Samojłowicz, M. Bieniek, K. Grela, *Chem. Rev.* **2009**, *109*, 3708–3742; c) G. C. Vougioukalakis, R. H. Grubbs, *Chem. Rev.* **2010**, *110*, 1746–1787.
- [3] For recent examples, see: a) S. Blechert, M. Schuster, *Angew. Chem.* **1997**, *109*, 2124–2144; *Angew. Chem. Int. Ed. Engl.* **1997**, *36*, 2036–2056; b) A. Fürstner, *Top. Catal.* **1997**, *4*, 285–299; c) Z. Yang, Y. He, D. Vourloumis, H. Vallberg, K. C. Nicolaou, *Angew. Chem.* **1997**, *109*, 170–172; *Angew. Chem. Int. Ed. Engl.* **1997**, *36*, 166–168; d) R. H. Grubbs, S. Chang, *Tetrahedron* **1998**, *54*, 4413–4450; e) S. F. Martin, J. M. Humphrey, A. Ali, M. C. Hillier, *J. Am. Chem. Soc.* **1999**, *121*, 866–867; f) M. E. Maier, *Angew. Chem.* **2000**, *112*, 2153–2157; *Angew. Chem. Int. Ed.* **2000**, *39*, 2073–2077; g) J. M. Humphrey, A. Liao, T. Rein, Y.-L. Wong, H.-J. Chen, A. K. Courtney, S. F. Martin, *J. Am. Chem. Soc.* **2002**, *124*, 8584–8592; h) J. Prunet, *Angew. Chem.* **2003**, *115*, 2932–2936; *Angew. Chem. Int. Ed.* **2003**, *42*, 2826–2830; i) M. L. Ferguson, D. J. O'Leary, R. H. Grubbs, *Org. Synth.* **2003**, *80*, 85–88; j) M. W. B. Pfeiffer, A. J. Phillips, *J. Am. Chem. Soc.* **2005**, *127*, 5334–5335; k) A. Gradillas, J. Pèrez-Castells, *Angew. Chem.* **2006**, *118*, 6232–6247; *Angew. Chem. Int. Ed.* **2006**, *45*, 6086–6100; l) D. E. White, I. C. Stewart, R. H. Grubbs, B. M. Stoltz, *J. Am. Chem. Soc.* **2008**, *130*, 810–811; m) J. E. Enquist, Jr., B. M. Stoltz, *Nature* **2008**, *453*, 1228–1231.
- [4] a) S. T. Nguyen, L. K. Johnson, R. H. Grubbs, J. W. Ziller, *J. Am. Chem. Soc.* **1992**, *114*, 3974–3975; b) S. T. Nguyen, R. H. Grubbs, J. W. Ziller, *J. Am. Chem. Soc.* **1993**, *115*, 9858–9859; c) P. Schwab, R. H. Grubbs, J. W. Ziller, *J. Am. Chem. Soc.* **1996**, *118*, 100–110.
- [5] a) T. Weskamp, W. C. Schattenmann, M. Spiegler, W. A. Hermann, *Angew. Chem.* **1998**, *110*, 2631–2633; *Angew. Chem. Int. Ed.* **1998**, *37*, 2490–2493; b) M. Scholl, S. Ding, C. W. Lee, R. H. Grubbs, *Org. Lett.* **1999**, *1*, 953–956; c) T. Weskamp, F. J. Kohl, W. Hieringer, D. Gleich, W. A. Hermann, *Angew. Chem.* **1999**, *111*, 2573–2576; *Angew. Chem. Int. Ed.* **1999**, *38*, 2416–2419; d) J. Huang, E. D. Stevens, S. P. Nolan, J. L. Peterson, *J. Am. Chem. Soc.* **1999**, *121*, 2674–2678.
- [6] a) S. B. Garber, J. S. Kingsbury, B. L. Gray, A. H. Hoveyda, *J. Am. Chem. Soc.* **2000**, *122*, 8168–8179; b) S. Gessler, S. Randl, S. Blechert, *Tetrahedron Lett.* **2000**, *41*, 9973–9976.
- [7] For examples of Ru metathesis catalysts bearing modified NHCs, see reference [2]; recent representative examples: a) T. Savoie, B. Stenne, S. K. Collins, *Adv. Synth. Catal.* **2009**, *351*, 1826–1832; b) L. Vieille-Petit, X. Luan, M. Gatti, S. Blumentritt, A. Linden, H. Clavier, S. P. Nolan, R. Dorta, *Chem. Commun.* **2009**, 3783–3785; c) S. Tiede, A. Berger, D. Schlesiger, D. Rost, A. Lühl, S. Blechert, *Angew. Chem.* **2010**, *122*, 4064–4067; *Angew. Chem. Int. Ed.* **2010**, *49*, 3972–3975; d) B. K. Keitz, R. H. Grubbs, *Organometallics* **2010**, *29*, 403–408.
- [8] L. Vieille-Petit, H. Clavier, A. Linden, S. Blumentritt, S. P. Nolan, R. Dorta, *Organometallics* **2010**, *29*, 775–788.
- [9] J. M. Berlin, K. Campbell, T. Ritter, T. W. Funk, A. Chlenov, R. H. Grubbs, *Org. Lett.* **2007**, *9*, 1339–1342.
- [10] I. C. Stewart, T. Ung, A. A. Pletnev, J. M. Berlin, R. H. Grubbs, Y. Schrodi, *Org. Lett.* **2007**, *9*, 1589–1592.
- [11] C. K. Chung, R. H. Grubbs, *Org. Lett.* **2008**, *10*, 2693–2696.
- [12] K. M. Kuhn, J.-B. Bourg, C. K. Chung, S. C. Virgil, R. H. Grubbs, *J. Am. Chem. Soc.* **2009**, *131*, 5313–5320.
- [13] F. Grisi, C. Costabile, E. Gallo, A. Mariconda, C. Tedesco, P. Longo, *Organometallics* **2008**, *27*, 4649–4656.
- [14] F. Grisi, A. Mariconda, C. Costabile, V. Bertolasi, P. Longo, *Organometallics* **2009**, *28*, 4988–4995.
- [15] L. Cavallo, *J. Am. Chem. Soc.* **2002**, *124*, 8965–8973.
- [16] C. Costabile, L. Cavallo, *J. Am. Chem. Soc.* **2004**, *126*, 9592–9600.
- [17] a) C. Adlhart, P. Chen, *J. Am. Chem. Soc.* **2004**, *126*, 3496–3510; b) B. F. Straub, *Angew. Chem.* **2005**, *117*, 6129–6132; *Angew. Chem. Int. Ed.* **2005**, *44*, 5974–5978.
- [18] A. Correa, L. Cavallo, *J. Am. Chem. Soc.* **2006**, *128*, 13352–13353.
- [19] C. N. Rowley, E. F. van der Eide, W. E. Piers, T. K. Woo, *Organometallics* **2008**, *27*, 6043–6045.
- [20] S. Fomine, M. A. Tlenkopatchev, *Organometallics* **2010**, *29*, 1580–1587.
- [21] F. Ragone, A. Poater, L. Cavallo, *J. Am. Chem. Soc.* **2010**, *132*, 4249–4258.
- [22] X. Solans-Monfort, R. Pleixats, M. Sodupe, *Chem. Eur. J.* **2010**, *16*, 7331–7343.
- [23] ORTEP III, Report ORNL-6895, M. N. Burnett, C. K. Johnson, Oak Ridge National Laboratory, Oak Ridge, **1996**.
- [24] a) M. Nishio, *Top. Stereochem.* **2006**, *25*, 255–302; b) M. Nishio, Y. Umezawa, K. Honda, S. Tsuboyama, H. Suezawa, *CrystEngComm* **2009**, *11*, 1757–1788.
- [25] a) T. Steiner, *Angew. Chem.* **2002**, *114*, 50–80; *Angew. Chem. Int. Ed.* **2002**, *41*, 48–76; b) A. Kovacs, Z. Varga, *Coord. Chem. Rev.* **2006**, *250*, 710–727.
- [26] K. Weigl, K. Köhler, S. Dechert, F. Meyer, *Organometallics* **2005**, *24*, 4049–4056.
- [27] T. Ritter, M. W. Day, R. H. Grubbs, *J. Am. Chem. Soc.* **2006**, *128*, 11768–11769.
- [28] M. Barbasiewicz, M. Bieniek, A. Michrowska, A. Szadkowska, A. Makal, K. Wozniak, K. Grela, *Adv. Synth. Catal.* **2007**, *349*, 193–203.
- [29] G. C. Vougioukalakis, R. H. Grubbs, *Organometallics* **2007**, *26*, 2469–2472.
- [30] E. Tzur, A. Ben-Asuly, C. E. Diesendruck, I. Goldberg, N. G. Lemcoff, *Angew. Chem.* **2008**, *120*, 6522–6525; *Angew. Chem. Int. Ed.* **2008**, *47*, 6422–6425.
- [31] S. L. Balof, S. J. P'Pool, N. J. Berger, E. J. Valente, A. M. Shiller, H.-J. Schanz, *Dalton Trans.* **2008**, 5791–5799.
- [32] H. Clavier, S. P. Nolan, M. Mauduit, *Organometallics* **2008**, *27*, 2287–2292.
- [33] D. Rix, F. Cajo, I. Laurent, F. Boeda, H. Clavier, S. P. Nolan, M. Mauduit, *J. Org. Chem.* **2008**, *73*, 4225–4228.
- [34] G. C. Vougioukalakis, R. H. Grubbs, *Chem. Eur. J.* **2008**, *14*, 7545–7556.
- [35] a) M. S. Sanford, M. Ulman, R. H. Grubbs, *J. Am. Chem. Soc.* **2001**, *123*, 749–750; b) M. S. Sanford, J. A. Love, R. H. Grubbs, *J. Am. Chem. Soc.* **2001**, *123*, 6543–6544.
- [36] J. A. Love, M. S. Sanford, M. W. Day, R. H. Grubbs, *J. Am. Chem. Soc.* **2003**, *125*, 10103–10109.
- [37] T. Vorfalt, K.-J. Wannowius, H. Plenio, *Angew. Chem.* **2010**, *122*, 5665–5668; *Angew. Chem. Int. Ed.* **2010**, *49*, 5533–5536.
- [38] T. Ritter, A. Hejl, A. G. Wenzel, T. W. Funk, R. H. Grubbs, *Organometallics* **2006**, *25*, 5740–5745.
- [39] As expected, phosphine-free catalysts **9a**, **9b**, **10a** and **10b** showed low activity in the RCM of **19** at 30°C. Among them, complex **9a** emerges as the most effective and requires 12 h to attain >95%

- yield. Under the same reaction condition, complex **4**, which is also a very efficient catalyst for hindered olefin formation, requires 15 h to produce cycloalkene **20** in 95 % yield.^[11]
- [40] a) T. Vorfalt, S. Leuthäuser, H. Plenio, *Angew. Chem.* **2009**, *121*, 5293–5296; *Angew. Chem. Int. Ed.* **2009**, *48*, 5191–5194; b) V. Sashuk, L. H. Peeck, H. Plenio, *Chem. Eur. J.* **2010**, *16*, 3983–3993.
- [41] D. Rost, M. Porta, S. Gessler, S. Blechert, *Tetrahedron Lett.* **2008**, *49*, 5968–5971.
- [42] C. Samojłowicz, M. Bieniek, A. Zarecki, R. Kadirov, K. Grela, *Chem. Commun.* **2008**, 6282–6284.
- [43] a) T. J. Seiders, D. W. Ward, R. H. Grubbs, *Org. Lett.* **2001**, *3*, 3225–3228; b) T. W. Funk, J. M. Berlin, R. H. Grubbs, *J. Am. Chem. Soc.* **2006**, *128*, 1840–1846.
- [44] I. C. Stewart, D. Benitez, D. J. O’Leary, E. Tkatchouk, M. W. Day, W. A. Goddard, R. H. Grubbs, *J. Am. Chem. Soc.* **2009**, *131*, 1931–1938.
- [45] E. F. Van der Eide, W. E. Piers, *Nat. Chem.* **2010**, *2*, 571–576.
- [46] E. F. Van der Eide, P. E. Romero, W. E. Piers, *J. Am. Chem. Soc.* **2008**, *130*, 4485–4491.
- [47] I. C. Stewart, B. K. Keitz, K. M. Kuhn, R. M. Thomas, R. H. Grubbs, *J. Am. Chem. Soc.* **2010**, *132*, 8534–8535.
- [48] J. Louie, R. H. Grubbs, *Organometallics* **2002**, *21*, 2153–2164.

Received: February 12, 2011

Revised: March 18, 2011

Published online: June 15, 2011